


Research Article

Cryo-EM structure of the *Rhodospirillum rubrum* RC–LH1 complex at 2.5 Å

Pu Qian^{1,2}, Tristan I. Croll³, David J.K. Swainsbury², Pablo Castro-Hartmann¹, Nigel W. Moriarty⁴, Kasim Sader¹ and  C. Neil Hunter²

¹Materials and Structural Analysis, Thermo Fisher Scientific, Achtseweg Noord 5, 5651 GG Eindhoven, Netherlands; ²Department of Molecular Biology and Biotechnology, University of Sheffield, Sheffield, U.K.; ³Cambridge Institute for Medical Research, University of Cambridge, Cambridge CB2 0XY, U.K.; ⁴Molecular Biophysics and Integrated Bio-imaging, Lawrence Berkeley National Laboratory, Berkeley, CA 94720, U.S.A

Correspondence: C. Neil Hunter (c.n.hunter@sheffield.ac.uk)



The reaction centre light-harvesting 1 (RC–LH1) complex is the core functional component of bacterial photosynthesis. We determined the cryo-electron microscopy (cryo-EM) structure of the RC–LH1 complex from *Rhodospirillum rubrum* at 2.5 Å resolution, which reveals a unique monomeric bacteriochlorophyll with a phospholipid ligand in the gap between the RC and LH1 complexes. The LH1 complex comprises a circular array of 16 $\alpha\beta$ -polypeptide subunits that completely surrounds the RC, with a preferential binding site for a quinone, designated Q_P, on the inner face of the encircling LH1 complex. Quinols, initially generated at the RC Q_B site, are proposed to transiently occupy the Q_P site prior to traversing the LH1 barrier and diffusing to the cytochrome *bc*₁ complex. Thus, the Q_P site, which is analogous to other such sites in recent cryo-EM structures of RC–LH1 complexes, likely reflects a general mechanism for exporting quinols from the RC–LH1 complex.

Introduction

Reaction centre-light harvesting complex 1 (RC–LH1) complexes are the central functional units of photosynthesis in purple phototrophic bacteria. Solar energy absorbed by a circular LH1 assembly migrates to an enclosed membrane-bound RC [1], where a succession of charge separation and protonation events produces a quinol that leaves the RC–LH1 complex, carrying protons and electrons to a cytochrome (cyt) *bc*₁ complex [2,3]. The LH1 complex is formed from an oligomeric assembly of transmembrane $\alpha\beta$ heterodimers, which bind bacteriochlorophyll (BChl) and carotenoid pigments and curve round the central RC complex. In some phototrophic bacteria, the ring of LH1 subunits is incomplete and the ‘missing’ LH1 $\alpha\beta$ subunits create a gap through which quinones and quinols can enter and leave the RC–LH1 complex to sustain repeated turnovers of the photosystem. In such complexes one or more transmembrane polypeptides forms part of this interrupted LH1 assembly [4–7]. In other RC–LH1 complexes the RC is fully encircled by LH1 and there is no obvious entry and exit point for quinone traffic [8–10]. Structures of these complexes have revealed small pores in the LH1 antenna that are apparently sufficient to allow the passage of quinones across the LH1 barrier. One such complex, from the phototrophic bacterium *Rhodospirillum (Rsp.) rubrum*, has been particularly well-studied over many years, with the lack of detailed structural information for this RC–LH1 complex at odds with its important roles in studies of energy transfer [11–13], carotenoid function [14–16] and *in vitro* LH1 assembly [17–19]. Furthermore, more detailed structural data are required to augment earlier NMR work [20] as well as structural information from cryo-electron microscopy (cryo-EM) and atomic force microscopy studies of 2-D crystals [21–24]. A high-resolution structure would also address some intriguing and unsolved aspects of the *Rsp. rubrum* RC–LH1 complex, which include the use of geranylgeraniol (GG) and phytol to esterify the BChl and bacteriopheophytin (BPhe) pigments, respectively [25,26], the shape of the complex that likely imparts curvature on the

Received: 6 July 2021
 Revised: 12 August 2021
 Accepted: 17 August 2021

Accepted Manuscript online:
 17 August 2021
 Version of Record published:
 7 September 2021

intracytoplasmic membrane [27,28], and the potentially problematic, continuous LH1 barrier round the *Rsp. rubrum* RC that nevertheless allows rapid quinone traffic between the RC and cyt *bc*₁ complexes [29].

Here, we used cryo-EM to determine the structure of the RC–LH1 complex from *Rsp. rubrum* at 2.5 Å resolution, which shows the detailed organization of all protein and cofactor components, a preferential site for quinone diffusion across the fully circular LH1 complex, and a unique monomeric BChl, with a phospholipid ligand, in the gap between the RC and LH1 complexes.

Materials and methods

Cell culture and protein purification

Wild type cells of *Rsp. rubrum* strain S1 were cultured photosynthetically in M22+ medium under illumination (100 μmol of photons m⁻² s⁻¹) at 30°C in 20 L screw-capped vessels. When the culture reached an absorbance at 680 nm of 1.6 cells were harvested by centrifugation at 3290g for 30 min. The harvested cells were washed using working buffer (20 mM HEPES, pH 7.8). Washed cells were suspended in the working buffer with a few grains of DNase and MgCl₂ and broken by three passages through a French Press at 18 000 psi. The broken cell suspension was applied to a two-step sucrose gradient (15% and 40% (w/w) in a SW32 ultracentrifuge tube), and spun for 4 h at 100 000g. Photosynthetic membranes were collected at the 15%–40% sucrose interface and pelleted. After re-suspension in working buffer, the absorbance of the membrane solution was adjusted to ~100 at 880 nm. For solubilization of the core complexes, the absorbance at 880 nm of the photosynthetic membrane was adjusted to 60 (1 cm pathlength), and n-Dodecyl-β-D-Maltoside (β-DDM) was added to a final concentration of 3% (w/w). This mixture was then stirred in the dark at 4°C for 30 min. Unsolubilized material was removed by centrifugation for 1 h at 211 000g. The clarified supernatant was loaded onto an DEAE-Sepharose ion exchange column pre-equilibrated with running buffer (working buffer solution containing 0.03% β-DDM). The column was washed using 2 column volumes of running buffer followed by stepwise washing to 120 mM NaCl. A 100 ml gradient of 120–300 mM NaCl then was used to elute the complexes from the column. Fractions were monitored using an A880/A820 absorption ratio, and fractions with a ratio >2.0 were pooled, and concentrated for the next purification step on a Superdex 200 gel filtration column. Fractions with an A880/A820 absorbance ratio >2.2 were pooled and used for cryo-EM data collection.

Cryo-EM data collection

The protein concentration was adjusted to an absorbance of 100 at 880 nm. 3.0 μl protein solution was applied to a glow-discharged holey carbon grid (Quantifoil grid R1.2/1.3, 300 mesh Cu). The grid was plunged into liquid ethane cooled by liquid nitrogen using a FEI Vitrobot 4. Parameters were set as following: blotting time 2.5 s, sample chamber humidity 99%, sample chamber temperature 4°C. The frozen grid was stored in liquid nitrogen before use. Data were recorded at the Cambridge Pharmaceutical Cryo-EM Consortium on a ThermoFisher Scientific Titan Krios G3i Cryo-Transmission Electron Microscope (Cryo-TEM) equipped with a Falcon 4 direct electron detector. The microscope was operated at 300 kV accelerating voltage, at a nominal magnification of 120 000×, corresponding to a pixel size of 0.65 Å at the specimen level. The detector was operated in counting mode. A total dose of 45 electrons per Å² was divided between 42 frames within 12.21 s exposure time, resulting in an electron dose of 1.07 e⁻/Å²/frame. In total, 9 024 movies were collected with defocus values varied from 0.8 to 2.2 μm. A typical cryo-EM image, averaged from motion corrected movie frames, is shown in Supplementary Figure S1A.

Data processing

Image processing was performed within RELION 3.1. Beam-induced movement of dose fractionated images were corrected using RELION's built-in motioncorr2 [30] on 5 × 5 patches. CTF parameters were determined using CTFIND4 [31]. In total, 1 519 688 particles were picked based on the particle coordinates calculated from cisTEM [32] with a box size of 380 × 380, corresponding to a 24.7 nm square. These particles were subjected to reference-free two-dimensional classification. 1 128 646 (74%) particles from good 2D classes were selected for 3D classification. The resulting good 2D classes were subjected to an initial 3D model calculation using EMAN2 [33] for maximum-likelihood-based 3D classification. The best 3D class out of four, containing 519 005 particles (34%), was selected for high resolution 3D reconstruction and refinement, resulting in a 3.2 Å resolution 3D map. After CTF refinement, including anisotropic magnification, beam-tilt, trefoil, fourth order aberration, per particle defocus and per-image astigmatism estimation, Bayesian polishing was performed with

the default parameters provided by RELION, improving the resolution of the 3D map to 2.7 Å. The selected particles for the 3D refinement were re-extracted using a 512 × 512 box size for a final CTF refinement and Bayesian polishing, producing a 2.5 Å resolution map.

Modeling and refinement

Initially, the crystal structure of the reaction centre from *Rhodobacter (Rba.) sphaeroides* (PDB 3I4D) was fitted to the cryo-EM map as a rigid body using the *fit in map* function of Chimera [34]. The polypeptides of the RC-H, RC-M and RC-L subunits were mutated according to those from *Rsp. rubrum* using COOT [35]. They were then manually adjusted and real space refined for both polypeptides and cofactors. For LH1, a single subunit of the LH1 complex, $\alpha\beta\text{BChl}_2\text{Car}$, was built based on structural similarity compared with the LH1 of *Thermochromatium (Tch.) tepidum* [36]. It was docked into the density map so that the two BChl *a* molecules in the model fitted comfortably into their density in the map. Amino acid sequences then were replaced with those from *Rps. rubrum*, and real space refined in COOT. This subunit was copied to the other 15 $\alpha\beta$ subunits, forming a closed LH1 ring. Real space refinement was performed on individual $\alpha\beta$ subunits. All-*trans* spirilloxanthin and ubiquinone-10 molecules (Q_B and Q_P) were also fitted into the density map independently using COOT.

Analysis of pigment composition shows that the major carotenoid in the core complex is spirilloxanthin [37]; BChl *a* is esterified by a GG tail [38], whereas BPhe is esterified by phytol. *Rsp. rubrum* contains two types of quinone, ubiquinone-10 and rhodoquinone-10 [39]. All-*trans* spirilloxanthin and 15-*cis* spirilloxanthin fitted well into the LH1 and RC, respectively. BChl a_{GG} was used for the LH1 BChl *a* pair, RC special pair and RC accessory BChl *a*. Based on the 2.5 Å resolution map, RC Q_A and Q_B and Q_P were assigned to UQ-10, whereas Q_F was assigned to RQ-10. In addition, two tetramyristoyl cardiolipin and two phosphatidylglycerol lipids were modeled into the map. Restraints for novel ligands were generated using eLBOW [40] with the ideal values for bonds and angles obtained from Mogul [41,42]. All of the LH1 subunits and ligands underwent real-space refinement using ISOLDE [43]. The final model was subjected to global refinement and minimization using PHENIX [44]. The final refinement statistics are summarized in Supplementary Table S1. The quality of fit for the structural model within the electron density map was validated using EMRinger [45].

Results and discussion

Overall structure of the RC–LH1 complex

In this study, we report the structure of *Rsp. rubrum* RC–LH1 complex at 2.5 Å, determined by cryo-EM. In total, 9,024 cryo-EM movies were recorded, from which 1 519 688 particles were picked for further data processing yielding a final resolution of 2.5 Å (Figure 1, Supplementary Figures S1, S2, Supplementary Table S1). The density map (Figure 1A–C) shows the overall shape of the complex, which is slightly elliptical in projection with short and long axes of 115 and 123 Å (Figure 1A), and 94 Å in height (Figure 1B). As Figure 1B also shows, the shape of the complex in the plane of the membrane is cylindrical, yet the chromatophore membranes of *Rsp. rubrum*, in which RC–LH1 complexes are the dominant complex [46], are curved with a ~50–100 nm diameter [27,28]. Only a few degrees of conical angle are required to account for this level of curvature, and we conclude that in the native membrane a ring of lipid molecules binds to the outer face of the LH1- β polypeptide on the cytoplasmic side of the complex. Inspection of the density map shows disordered detergent molecules in the position that lipids are suggested to occupy, and lipids bound tightly in these positions round the LH1 ring would confer a slight conical shape on the complex. There are precedents for bound, and structurally resolved, rings of lipids and detergents in RC–LH1 complexes from *Rhodopseudomonas (Rps.) palustris* (RC–LH1₁₄-W; Protein Data Bank (PDB) 6Z5S, and RC–LH1₁₆, 6Z5R) [6], *Rba. veldkampii* (7DDQ) [7], *Tch. tepidum* (5Y5S) [9] and *Thiorhodovibrio (Trv.)* strain 970 (7C9R) [10]. Ribbon models of the complex are shown in Figure 1D–F. Although the RC is completely surrounded by the LH1 complex only one H-bond connects the RC and the LH1 ring, between LH1- α 1 Ser34 and RC-H Trp9 (3.1 Å); we suggest that this point of contact is a potential site for initiating the assembly of a curved array of LH1 $\alpha\beta$ subunits that culminates in a fully encircled RC, so it is assigned as $\alpha\beta(1)$. Each of the 16 pairs of transmembrane α and β polypeptides, numbered in Figure 1D, binds two BChl a_{GG} molecules creating a ring of 32 closely spaced and paired BChl *a* pigments. In this respect, the *Rsp. rubrum* LH1 antenna is very similar to the 16-subunit ring of *Tch. tepidum* [9] and to the RC–LH1₁₆ complex of *Rps. palustris* [6].

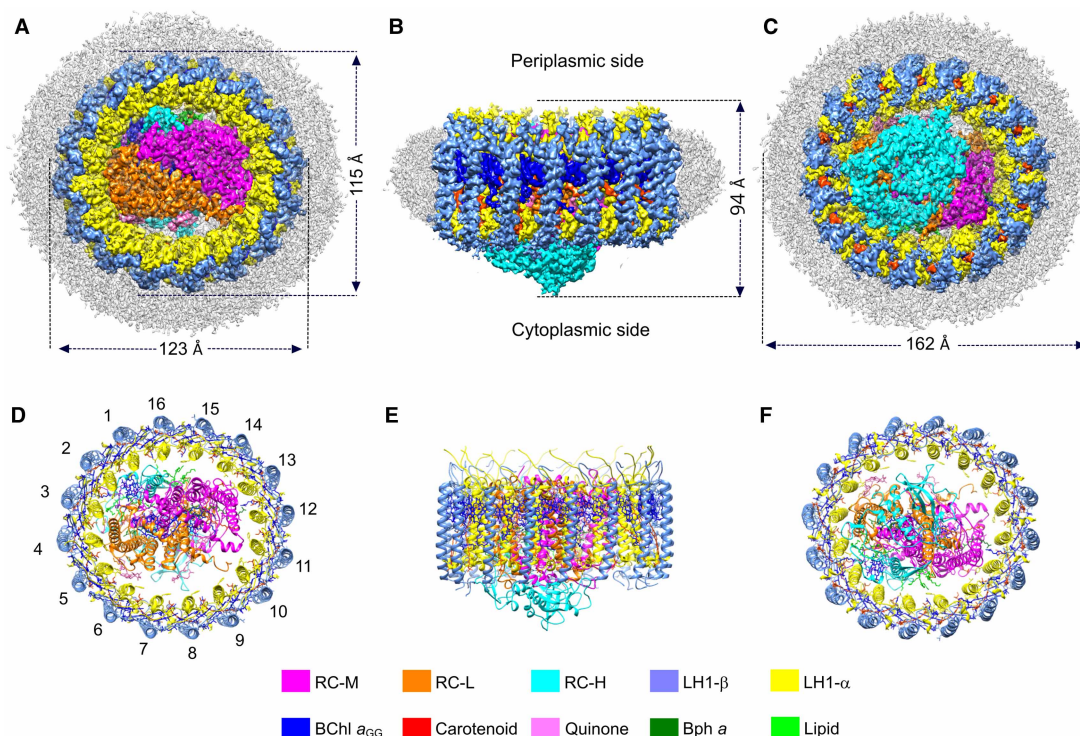


Figure 1. Cryo-EM structure of the RC–LH1 core complex from *Rsp. rubrum*.

(A–C) Views of the RC–LH1 density map, colored as in the key at the bottom of the figure. Detergent and other disordered molecules are in grey. (A) View of the slightly elliptical LH1 ring from the periplasmic side of the membrane, showing the diameters of the long and short axes. (B) View in the plane of the membrane showing the height of the complex. (C) Perpendicular view from the cytoplasmic side. (D–F) Ribbon models corresponding to (A–C), made using Chimera [58]; the LH1 subunits are numbered in (D).

Structure of the LH1 complex

The LH1 $\alpha\beta$ subunits are the building blocks of the LH1 ring; Figure 2A shows the structure of a single $\alpha\beta$ subunit, which is stabilized by a series of protein–protein, BChl–protein, BChl–BChl, carotenoid–BChl and carotenoid–protein contacts. LH1 α consists of a short N-terminal helix of nine residues that lies parallel to the surface of the membrane on the cytoplasmic side, followed by a transmembrane domain and a 14-residue C-terminal region that contains a loop structure. The LH1 β -polypeptide has the same topology as LH1 α . Hydrogen bonds between C- and N-terminal residues link the α and β polypeptides and contribute to the formation of LH1 $\alpha\beta$ subunits: α -Gln50– β -Asn53, 2.9 Å; α -Gln50– β -Trp55, 2.9 Å; α -Ala44– β -Arg46, 2.9 Å; α -Arg37– β -Arg46, 2.8 Å; α -Arg37– β -Pro47, 2.8 Å and α -Gln6– β -Ile12, 2.8 Å. However, the binding of BChl and carotenoid pigments, and the ensuing pigment–pigment interactions, are the major driving forces that create the LH1 $\alpha\beta$ (BChl) $_2$ units, which behave in a modular fashion that can form either open or closed rings [4–10], or, in some RC-minus mutants, ellipses, and spirals of variable size [47]. LH1 α His29 and LH1 β His39 supply the ligands (2.6 and 2.5 Å, respectively) for binding a pair of opposing, excitonically coupled BChls. These pigments are modeled with GG ‘tails’ (BChl a_{GG}) in the well-resolved density map (Supplementary Figure S2). As with other light-harvesting LH1 complexes, hydrogen bonds from C-terminal residues (LH1 α Trp40 and LH1 β Trp48) to BChl C3 acetyl groups (2.6 and 2.5 Å, respectively) tune the absorption properties of the bound BChls [48,49]. A combination of excitonic coupling within and between BChl dimers, together with hydrogen bonding to LH1- α and LH1- β aromatic side chains, redshifts the absorption from \sim 770 nm for monomeric BChl in solvent to 880 nm in the RC–LH1 complex. The progressive red-shifting of absorption, as more LH1 $\alpha\beta$ (BChl) $_2$ units associate, has been examined extensively using *in vitro* reconstitution approaches [17–19]. Some of these studies employed a carotenoid-free mixture of polypeptides and BChls, but the native complex necessarily binds carotenoids, both for harvesting light in the 450–550 nm region of the spectrum and

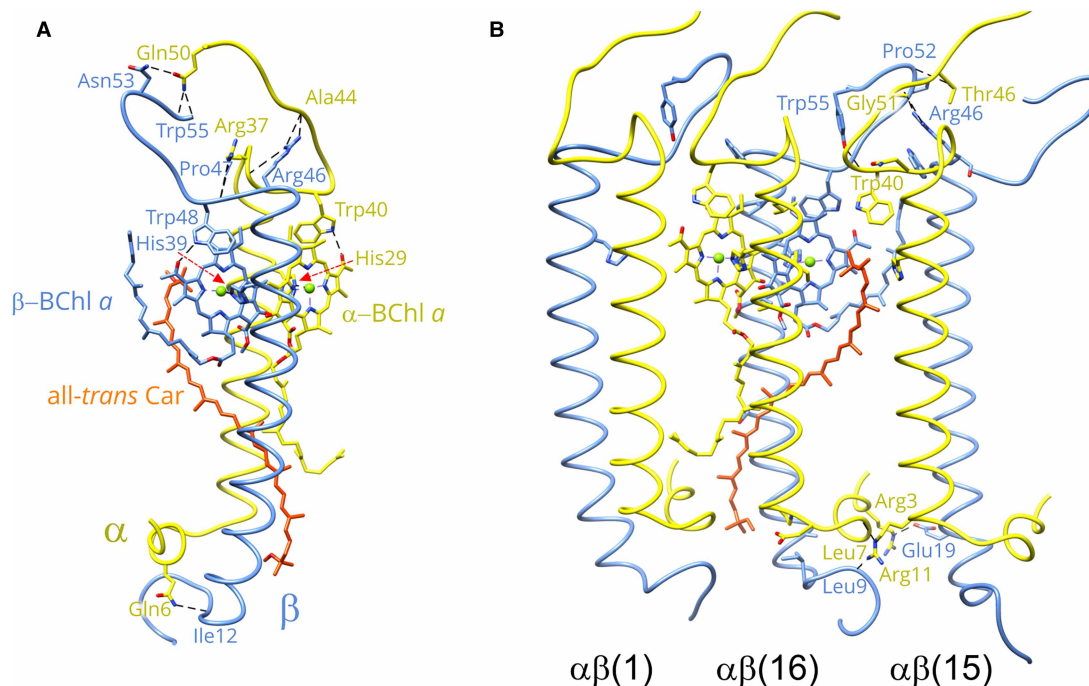


Figure 2. Protein–protein and protein–pigment interactions in the *Rsp. rubrum* RC–LH1 core complex.

(A) A single LH1 $\alpha\beta$ subunit, containing one α -polypeptide (yellow), one β -polypeptide (cornflower blue), two BChl a_{GG} molecules colored according to their cognate polypeptide, and one all-*trans* spirilloxanthin (red-orange). All residues involved in H-bonds are labelled. (B) Inter-subunit interactions between three adjoining LH1 $\alpha\beta$ subunits. Pigments are only shown in the middle subunit for clarity. Only residues involved in inter-subunit H-bonds are labelled.

for photoprotection. Many studies of excited state dynamics have focused on the *Rsp. rubrum* LH1 complex, for example [11–14], but the location and conformation of the carotenoid, spirilloxanthin, have remained unknown. Here, the structure of the RC–LH1 complex shows that the spirilloxanthins in the LH1 ring are in the all-*trans* configuration, making contacts with the N-terminal helical region ($\alpha 3$ -RIWQLF) of the $n - 1$ α -polypeptide and the transmembrane region ($\alpha 26$ -LLIHFIILL) of the $n + 1$ α -polypeptide. The central region of the spirilloxanthin is in close contact (4.2 Å) with the tail of the α -BChl a_{GG} (Figure 2B). The extent of these contacts reveals a third, stabilizing, role for the carotenoid, analogous to the same role for these pigments in LH2 complexes [50,51]. Thus, carotenoids stabilize individual LH1 $\alpha\beta$ subunits, and interactions between spirilloxanthins and $n + 1$, n , $n - 1$ polypeptides interlock LH1 $\alpha\beta$ subunits and promote the formation of a curved, oligomeric assembly. A subset of this interlocking ring structure is shown in Figure 2B, in which hydrogen-bonds help to stabilize associations between adjacent LH1 $\alpha\beta$ subunits. Focusing on subunits 15 and 16, at the periplasmic (C-terminal) side of the complex these bonds are between $\beta(15)$ -Gly51 and $\beta(16)$ -Arg46, 3.0 Å; $\beta(15)$ -Pro52 and $\alpha(16)$ -Thr46, 3.3 Å; $\beta(15)$ -Tyr55 and $\alpha(16)$ -Trp40, 2.6 Å. On the N-terminal side there are hydrogen bonds between $\alpha(15)$ -Glu19 and $\beta(16)$ -Arg3, 2.8 Å; $\alpha(15)$ -Leu7 and $\alpha(16)$ -Arg11, 2.8 Å; $\beta(15)$ -Leu9 and $\alpha(16)$ -Arg11, 2.8 Å.

The reaction centre, and the space between this complex and LH1

The RC consists of H, M and L subunits (Figure 1, Supplementary Figure S2), and the internal arrangement of BChl, bacteriopheophytin (BPhe), carotenoid (Car), quinone and Fe cofactors is shown in Figure 3A. Supplementary Figure S2 shows the quality of fits of atomic models for all the cofactors and protein components to their respective densities within the 2.5 Å resolution map. The unusual presence of both GG and phytol ‘tails’ of the various RC pigments in *Rsp. rubrum* has been known for many years [25]. BChl a esterified with a GG tail (Supplementary Figure S3), BChl a_{GG} , was used in our structural model for the RC special pair and accessory BChl pigments; the BPhe pigments are esterified with phytol. Surprisingly, we identified an extra BChl a_{GG} , localized between the second LH1 $\alpha\beta$ subunit and the RC special pair (Figure 3A). This pigment is

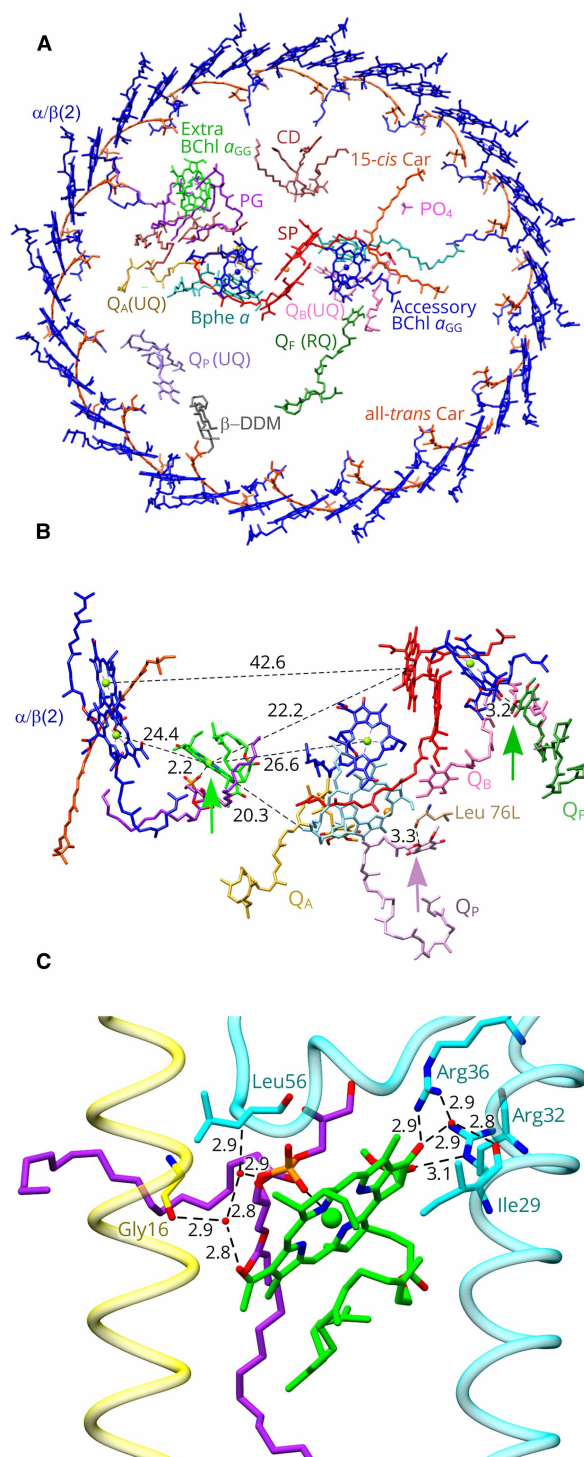


Figure 3. Arrangement of pigments and cofactors in the *Rsp. rubrum* RC-LH1 core complex.

Part 1 of 2

(A) Perpendicular view from the periplasmic side of the membrane. Water molecules were omitted for clarity. PG, Phosphatidyl glycerol; CD, cardiolipin; SP, the reaction centre special pair of BChl a_{GG} molecules. (B) Location and pigment environment of the extra BChl a_{GG} (bright green; colours as in panel (A)). The central Mg ion of this BChl a_{GG} is coordinated by the nearby PG lipid molecule, indicated by a bright green arrow. A lone pair π interaction between Q_P and RC-L Leu 76 is indicated with a mauve arrow, and a mid-green arrow points to a lone pair π interaction between non-protein bound rhodoquinone RQ and the accessory BChl a_{GG} on the B-branch of the RC. (C) Detailed view of the bonding environment for the extra BChl a_{GG} (green).

Figure 3. Arrangement of pigments and cofactors in the *Rsp. rubrum* RC–LH1 core complex.

Part 2 of 2

Three water molecules are shown as small red spheres, with hydrogen bonds shown as dashed lines with the distances in Ångstroms indicated. LH1 α is in yellow, The RC-H subunit is in cyan, and the PG is in magenta.

not bound to a protein, and instead it is coordinated by an oxygen within the headgroup of a neighboring phosphatidylglycerol molecule. This type of coordination has not been observed before in RC–LH1 complexes, but in the RC from the green sulfur bacterium *Chlorobaculum tepidum* [52] it has been proposed that the headgroup of a phosphatidylglycerol molecule coordinates a water molecule forming the axial ligand of the A0 Chl *a* [53]. One of the acyl chains of the RC–LH1 lipid is close to the GG tail of a BChl bound to the α -polypeptide of LH1 $\alpha\beta(2)$ and to a spirilloxanthin molecule (Supplementary Figure S4). Presumably the interactions between LH1, a lipid, and the extra BChl are sufficient to position this pigment consistently, so it becomes a defined feature in the density map.

The function of this BChl a_{GG} pigment, unique in currently determined RC–LH1 structures, is unknown. Figure 3 displays the distances to neighboring pigments, showing that the extra BChl a_{GG} is located approximately midway between the BChl a_{GG} pair attached to LH1 $\alpha\beta(2)$ and the RC special pair of BChl a_{GG} pigments, a distance of 42.6 Å, with its macrocycle tilted $\sim 60^\circ$ from the special pair. The distance from the special pair is 22.2 Å, and 26.6 Å separates the extra BChl a_{GG} from the accessory BChl a_{GG} on the active (A branch) of the bifurcated network of RC cofactors. In the context of the inverse sixth power distance dependence for Förster energy transfer [54], halving the gap between the LH1 donor and RC acceptor pigments could exert a significant effect on LH1 to RC transfer. However, the absorption maximum of this pigment is also a factor to consider. Figure 3C shows the environment of this extra BChl a_{GG} which, in addition to its ligand with the nearby phosphatidyl glycerol (magenta), forms a series of hydrogen bonds with the RC H-subunit and with the second LH1 α subunit. The C13² ester of this BChl a_{GG} hydrogen-bonds to RCH–Arg32 NE, and the C13¹ keto bonds to RCH–Arg36. In addition, three water molecules (small red spheres in Figure 3C) form a hydrogen bond network between the C3-acetyl of BChl a_{GG} , the backbone oxygen of LH1 α –Gly16, the lipid and the backbone N of RCH–Leu56. Finally, there is also a water bridging to the RCH–Ile29 OH. As a monomeric pigment, the absorption maximum of this extra BChl a_{GG} is likely to be ~ 800 nm by analogy with, for example, LH2 complexes [55,56]. A protein engineering study was conducted on the β -Arg30 residue near to the monomeric B800 BChl in the LH2 complex of *Rba. sphaeroides*. Raman spectroscopy of β -Arg30 mutants showed that the loss of a hydrogen bond to the C3-acetyl group, and it was concluded that the absorption red-shift attributable solely to the H-bond is ~ 10 nm [55]. Thus the absorption maximum of a monomeric BChl, ~ 780 nm in solvent, would likely absorb no further to the red than 800 nm and this is proposed to apply to the BChl a_{GG} in the *Rsp. rubrum* RC–LH1 complex. If this is the case, energy transfer from 880 nm LH1 BChls to this new BChl would be ‘uphill’; onward excitation transfer to the RC special pair absorbing at 865 nm would be correspondingly ‘downhill’, though, and energetically level to the accessory RC BChl absorbing near 800 nm. Overall, the extra BChl a_{GG} could act as a conduit for energy transfer to the RC, but early picosecond transient absorption experiments showed no difference between *Rsp. rubrum* and *Rba. sphaeroides* RC–LH1 complexes, with rates of energy transfer in the 30–40 ps range [12].

Four quinone molecules were identified: Q_A, Q_B and Q_P are assigned as ubiquinone-10, based on their well-resolved densities (Supplementary Figure S2). Both the RC Q_A and Q_B sites are occupied, and there is a clear density for another quinone that sits between the RC and the inner face of the LH1 complex. Despite the disorder presumed to exist in the space between the RC and LH1 complexes, we could assign a rhodoquinone-10 at a position designated Q_F (‘free’ quinone) based on the match between its chemical structure and the density shape (Figure 3A, Supplementary Figures S2, S3). ‘Free’ quinones, with no surrounding protein to provide a defined binding pocket, were also found in *Rps. palustris*, *Tch. tepidum* and *Rba. veldkampii* RC–LH1 complexes [6,7,9]. There is a lone pair π interaction between the head of Q_F and the C13¹ acetyl group of the accessory BChl a_{GG} on the B-branch.

In the *Rsp. rubrum* structure, there is one spirilloxanthin molecule per LH1 $\alpha\beta$ (BChl)₂ unit, and this stoichiometry has been proposed to create a series of pores round the LH1 ring that could allow passage of quinone across the LH1 ring by means of ‘breathing motions’ [29,55]. This view of quinone diffusion does not assign any particular location or set of LH1 subunits for traversing the LH1 ring. However, the *Rsp. rubrum* RC–LH1 structure adds to the lengthening list of complexes [5–10] that have a conserved Q_P quinone (Figure 4A). The head group of the Q_P quinone in the *Rsp. rubrum* LH1 makes lone pair π interactions with the backbone

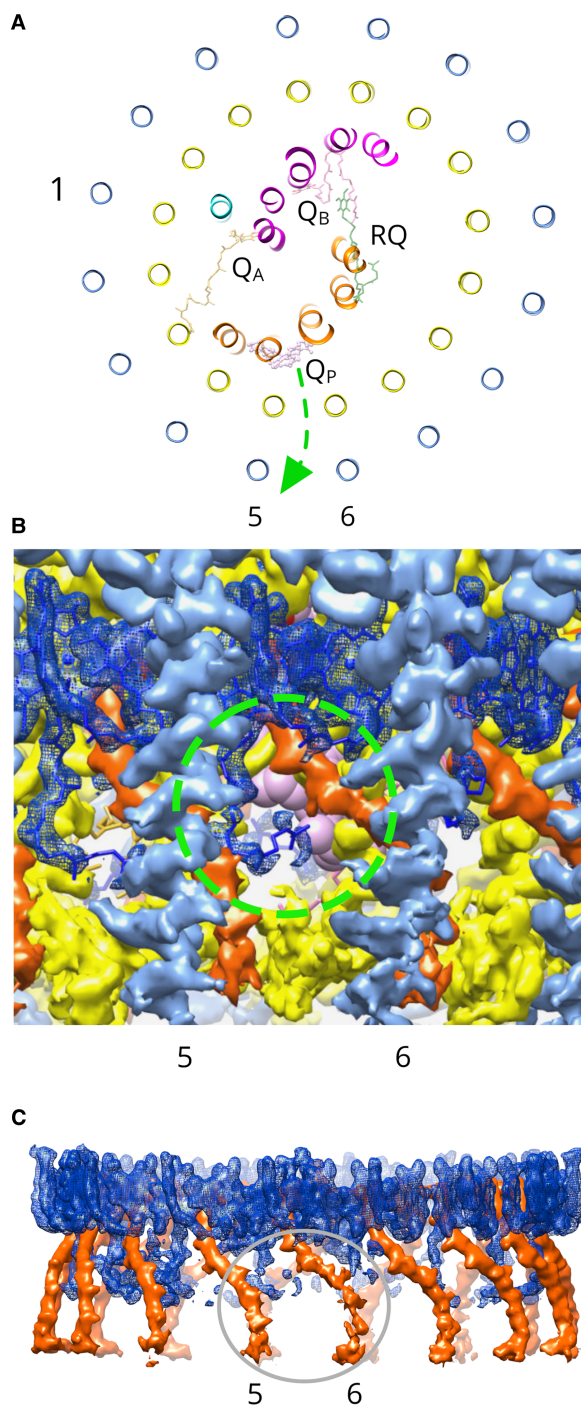


Figure 4. Location of a quinone/quinol channel adjacent to the Q_p site in the LH1 ring.

(A) The RC–LH1 complex viewed from the periplasmic side, with α -helices represented as ribbons and appearing as circles in the case of LH1 polypeptides. Only quinone cofactors are shown. Subunits are colored as in Figure 1. LH1- $\alpha\beta$ subunits 1, 5 and 6 are labeled. A green arrow indicates the proposed path taken by a quinol through the pore. (B) View of the LH1 complex in the plane of the membrane, from outside the complex. The LH1 α -polypeptide is in yellow, the β -polypeptide in cornflower blue, BChl a_{GG} molecules are blue, and the all-*trans* spirilloxanthin is in red-orange. The green dashed circle shows the pore, with the weak density of this particular GG tail allowing a view of the Q_p quinone (pink) visible in the background. (C) Densities of pigments adjacent to the LH1 pore. The grey ellipse delineates the weaker densities for the GG tail and the carotenoid at these positions in the LH1 ring.

oxygen of RC-L Leu 76, and the isoprenyl tail makes contacts with LH1 α 4 and 5. As with other such Q_P sites, we suggest that transient docking into this binding pocket prepares the quinone for passage through an adjacent pore between LH1 α β (BChl)₂ units. This does not rule out migration paths across other parts of the LH1 ring, although these routes may be less probable. In particular, we note the structurally resolved β -DDM detergent molecule (Figure 3A, grey), which fits well into the density near to Q_P (Supplementary Figure S5). This detergent molecule could have displaced a lipid, or a quinone, or it could sit in a pore in the LH1 ring between subunits 6 and 7, indicating another possible point of exit for quinol produced at the RC Q_B site.

The Q_P pore is circled in green in Figure 4B, and the Q_P quinone molecule can be seen by virtue of the weaker density for the GG tail of the BChl, relative to other pigments in the ring (Figure 4C). Similarly, the density for the cytoplasmic end of the spirilloxanthin in LH1 α β (6) is also weaker than for neighboring carotenoids. Counterparts of the Q_P quinone have been found in several RC–LH1 structures [5–10], and in each case Q_P associates with the inner face of the LH1 complex adjacent to a pore that would allow quinone movement across the LH1 ring. In the case of the *Blastochloris viridis* RC–LH1 [8], Q_P is adjacent to a region of relatively weak density for the BChl phytol and the associated carotenoid, which was proposed to reflect conformational flexibility leading to local disorder where quinones diffuse across the complex. We propose that transient occupation of the Q_P site increases the probability that the quinol will pass through the adjacent pore in the RC–LH1 complex of *Rsp. rubrum*.

Data Availability

The cryo-EM density map has been deposited in the World Wide Protein Data Bank (wwPDB) under accession code EMD-13110 and the coordinates have been deposited in the Protein Data Bank (PDB) under accession number 7OY8.

Competing Interests

The authors declare that there are no competing interests associated with the manuscript.

Funding

P.Q., D.J.K.S. and C.N.H. were supported by the Biotechnology and Biological Sciences Research Council (BBSRC) UK, award number BB/M000265/1, and C.N.H. and D.J.K.S. are supported by European Research Council Synergy Award 854126. T.I.C. acknowledges Wellcome Trust grant 209407/Z/17/Z.

Open Access Statement

Open access for this article was enabled by the participation of University of Sheffield in an all-inclusive *Read & Publish* pilot with Portland Press and the Biochemical Society under a transformative agreement with JISC.

CRedit Author Contribution

C. Neil Hunter: Conceptualization, Supervision, Funding acquisition, Writing — original draft, Project administration, Writing — review and editing. **Pu Qian:** Conceptualization, Data curation, Formal analysis, Supervision, Validation, Investigation, Visualization, Methodology, Writing — original draft. **Tristan Ian Croll:** Software, Formal analysis, Validation, Methodology. **David JK Swainsbury:** Visualization, Writing — review and editing. **Pablo Castro-Hartmann:** Investigation. **Nigel W. Moriarty:** Formal analysis. **Kasim Sader:** Investigation.

Acknowledgements

We acknowledge the European Synchrotron Radiation Facility for provision of initial beam time on CM01 (MX-2117) and we would like to thank Dr. Michael Hons for his assistance.

Abbreviations

β -DDM, n-Dodecyl- β -D-Maltoside; BChl a_{GG} , BChl *a* esterified with a GG tail; BChl, Bacteriochlorophyll *a*; BPhe, bacteriopheophytin; cryo-EM, cryo-electron microscopy; GG, geranylgeraniol; *Rba.*, *Rhodobacter*; RC–LH1, reaction centre light-harvesting 1 complex; *Rps.*, *Rhodospseudomonas*; *Rsp.*, *Rhodospirillum*; *Tch.*, *Thermochromatium*; *Trv.*, *Thiorhodovibrio*.

References

- 1 Gardiner, A.T., Nguyen-Phan, T.C. and Cogdell, R.J. (2020) A comparative look at structural variation among RC-LH1 'Core' complexes present in anoxygenic phototrophic bacteria. *Photosynth. Res.* **145**, 83–96 <https://doi.org/10.1007/s11120-020-00758-3>

- 2 Sener, M., Strumpfer, J., Singharoy, A., Hunter, C.N. and Schulten, K. (2016) Overall energy conversion efficiency of a photosynthetic vesicle. *eLife* **5**, e09541 <https://doi.org/10.7554/eLife.09541>
- 3 Singharoy, A., Maffeo, C., Delgado-Magnero, K.H., Swainsbury, D.J.K., Sener, M., Kleinekathofer, U. et al. (2019) Atoms to phenotypes: molecular design principles of cellular energy metabolism. *Cell* **179**, 1098–1111.e23 <https://doi.org/10.1016/j.cell.2019.10.021>
- 4 Qian, P., Papiz, M.Z., Jackson, P.J., Brindley, A.A., Ng, I., Olsen, J.D. et al. (2013) The 3-D structure of the *Rhodobacter sphaeroides* RC-LH1-PufX complex: dimerization and quinone channels promoted by PufX. *Biochemistry* **52**, 7575–7585 <https://doi.org/10.1021/bi4011946>
- 5 Xin, Y., Shi, Y., Niu, T., Wang, Q., Niu, W., Huang, X. et al. (2018) Cryo-EM structure of the RC-LH core complex from an early branching photosynthetic prokaryote. *Nat. Commun.* **9**, 1568 <https://doi.org/10.1038/s41467-018-03881-x>
- 6 Swainsbury, D.J.K., Qian, P., Jackson, P.J., Faries, K.M., Niedzwiedzki, D., Martin, E.C. et al. (2021) Structures of *Rhodopseudomonas palustris* RC-LH1 complexes with open or closed quinone channels. *Sci. Adv.* **7**, eabe2631 <https://doi.org/10.1126/sciadv.abe2631>
- 7 Bracun, L., Yamagata, A., Christianson, B.M., Terada, T., Canniffe, D.P., Shirouzu, M. et al. (2021) Cryo-EM structure of the photosynthetic RC-LH1-PufX supercomplex at 2.8-Å resolution. *Sci. Adv.* **7**, eabf8864 <https://doi.org/10.1126/sciadv.abf8864>
- 8 Qian, P., Siebert, C.A., Wang, P.Y., Canniffe, D.P. and Hunter, C.N.C. (2018) Cryo-EM structure of the *Blastochloris viridis* LH1-RC complex at 2.9 Å. *Nature* **556**, 203–208 <https://doi.org/10.1038/s41586-018-0014-5>
- 9 Yu, L.J., Suga, M., Wang-Otomo, Z.Y. and Shen, J.R. (2018) Structure of photosynthetic LH1-RC supercomplex at 1.9 Å resolution. *Nature* **556**, 209–213 <https://doi.org/10.1038/s41586-018-0002-9>
- 10 Tani, K., Kanno, R., Makino, Y., Hall, M., Takenouchi, M., Imanishi, M. et al. (2020) Cryo-EM structure of a Ca²⁺-bound photosynthetic LH1-RC complex containing multiple αβ-polypeptides. *Nat. Commun.* **11**, 4955 <https://doi.org/10.1038/s41467-020-18748-3>
- 11 Valkunas, L., Akesson, E., Pullerits, T. and Sundström, V. (1996) Energy migration in the light-harvesting antenna of the photosynthetic bacterium *Rhodospirillum rubrum* studied by time-resolved excitation annihilation at 77K. *Biophys. J.* **70**, 2373–2379 [https://doi.org/10.1016/S0006-3495\(96\)79804-1](https://doi.org/10.1016/S0006-3495(96)79804-1)
- 12 Visscher, K.J., Bergström, H., Sundström, V., Hunter, C.N. and van Grondelle, R. (1989) Temperature dependence of energy transfer from the long wavelength antenna bchl-896 to the reaction center in *Rhodospirillum rubrum*, *Rhodobacter sphaeroides* (w.t. and M21 mutant) from 77 to 177 K, studied by picosecond absorption spectroscopy. *Photosynth. Res.* **22**, 211–217 <https://doi.org/10.1007/BF00048300>
- 13 Kosumi, D., Maruta, S., Horibe, T., Fujii, R., Sugisaki, M., Cogdell, R.J. et al. (2011) Ultrafast energy-transfer pathway in a purple-bacterial photosynthetic core antenna, as revealed by femtosecond time-resolved spectroscopy. *Angew. Chem. Int. Ed. Engl.* **50**, 1097–1100 <https://doi.org/10.1002/anie.201003771>
- 14 Gradinaru, C.C., Kennis, J.T., Papagiannakis, E., van Stokkum, I.H., Cogdell, R.J., Fleming, G.R. et al. (2001) An unusual pathway of excitation energy deactivation in carotenoids: singlet-to-triplet conversion on an ultrafast timescale in a photosynthetic antenna. *Proc. Natl Acad. Sci. U.S.A.* **98**, 2364–2369 <https://doi.org/10.1073/pnas.051501298>
- 15 Akahane, J., Rondonuwu, F.S., Fiedor, L., Watanabe, Y. and Koyama, Y. (2004) Dependence of singlet energy transfer on the conjugation length of carotenoids reconstituted into the LH1 complex from *Rhodospirillum rubrum* G9. *Chem. Phys. Lett.* **393**, 184–191 <https://doi.org/10.1016/j.cplett.2004.06.021>
- 16 Nakagawa, K., Suzuki, S., Fujii, R., Gardiner, A.T., Cogdell, R.J., Nango, M. et al. (2008) Probing the effect of the binding site on the electrostatic behavior of a series of carotenoids reconstituted into the light-harvesting 1 complex from purple photosynthetic bacterium *Rhodospirillum rubrum* detected by Stark spectroscopy. *J. Phys. Chem. B* **112**, 9467–9475 <https://doi.org/10.1021/jp801773j>
- 17 Parkes-Loach, P.S., Sprinkle, J.R. and Loach, P.A. (1988) Reconstitution of the B873 light-harvesting complex of *Rhodospirillum rubrum* from the separately isolated α- and β-polypeptides and bacteriochlorophyll *a*. *Biochemistry* **27**, 2718–2727 <https://doi.org/10.1021/bi00408a011>
- 18 Davis, C.M., Bustamante, P.L. and Loach, P.A. (1995) Reconstitution of the bacterial core light-harvesting complexes of *Rhodobacter sphaeroides* and *Rhodospirillum rubrum* with isolated α- and β-polypeptides, bacteriochlorophyll *a* and carotenoid. *J. Biol. Chem.* **270**, 5793–5804 <https://doi.org/10.1074/jbc.270.11.5793>
- 19 Fiedor, L., Akahane, J. and Koyama, Y. (2004) Carotenoid-induced cooperative formation of bacterial photosynthetic LH1 complex. *Biochemistry* **43**, 16487–16496 <https://doi.org/10.1021/bi0481287>
- 20 Wang, Z.Y., Gokan, K., Kobayashi, M. and Nozawa, T. (2005) Solution structures of the core light-harvesting alpha and beta polypeptides from *Rhodospirillum rubrum*: implications for the pigment-protein and protein-protein interactions. *J. Mol. Biol.* **347**, 465–477 <https://doi.org/10.1016/j.jmb.2005.01.017>
- 21 Karrasch, S., Bullough, P.A. and Ghosh, R. (1995) The 8.5 Å projection map of the light-harvesting complex I from *Rhodospirillum rubrum* reveals a ring composed of 16 subunits. *EMBO J.* **14**, 631–638 <https://doi.org/10.1002/j.1460-2075.1995.tb07041.x>
- 22 Jamieson, S.J., Wang, P., Qian, P., Kirkland, J.Y., Conroy, M.J., Hunter, C.N. et al. (2002) Projection Structure of the photosynthetic reaction centre-antenna complex of *Rhodospirillum rubrum* at 8.5 Å resolution. *EMBO J* **21**, 3927–3935 <https://doi.org/10.1093/emboj/cdf410>
- 23 Qian, P., Adllessee, H.A., Ruban, A.V., Wang, P., Bullough, P.A. and Hunter, C.N. (2003) A reaction center – light harvesting 1 complex from a *Rhodospirillum rubrum* mutant with altered esterifying pigments: characterization by optical spectroscopy and cryo-electron microscopy. *J. Biol. Chem.* **278**, 23678–23685 <https://doi.org/10.1074/jbc.M302753200>
- 24 Fotiadis, D., Qian, P., Philippsen, A., Bullough, P.A., Engel, A. and Hunter, C.N. (2004) Structural analysis of the RC-LH1 photosynthetic core complex of *Rhodospirillum rubrum* using atomic force microscopy. *J. Biol. Chem.* **279**, 2063–2068 <https://doi.org/10.1074/jbc.M310382200>
- 25 Francke, C. and Amesz, J. (1995) The size of the photosynthetic unit in purple bacteria. *Photosynth. Res.* **46**, 347–352 <https://doi.org/10.1007/BF00020450>
- 26 Adllessee, H.A. and Hunter, C.N. (2002) *Rhodospirillum rubrum* possesses a variant of the *bchP* gene, encoding geranylgeranyl-bacteriopheophytin reductase. *J. Bacteriol.* **184**, 1578–1586 <https://doi.org/10.1128/JB.184.6.1578-1586.2002>
- 27 Vatter, A.E. and Wolfe, R.S. (1958) The structure of photosynthetic bacteria. *J. Bacteriol.* **75**, 480–488 <https://doi.org/10.1128/jb.75.4.480-488.1958>
- 28 Holt, S.C. and Marr, A.G. (1965) Isolation and purification of the intracytoplasmic membranes of *Rhodospirillum rubrum*. *J. Bacteriol.* **89**, 1413–1420 <https://doi.org/10.1128/jb.89.5.1413-1420.1965>
- 29 Aird, A., Wrachtrup, J., Schulten, K. and Tietz, C. (2007) Possible pathway for ubiquinone shuttling in *Rhodospirillum rubrum* revealed by molecular dynamics simulation. *Biophys. J.* **92**, 23–33 <https://doi.org/10.1529/biophysj.106.084715>

- 30 Zivanov, J., Nakane, T., Forsberg, B.O., Kimanius, D., Hagen, W.J.H., Lindahl, E. et al. (2018) New tools for automated high-resolution cryo-EM structure determination in RELION-3. *eLife* **7**, e42166 <https://doi.org/10.7554/eLife.42166>
- 31 Rohou, A. and Grigorieff, N. (2015) CTFIND4: fast and accurate defocus estimation from electron micrographs. *J. Struct. Biol.* **192**, 216–221 <https://doi.org/10.1016/j.jsb.2015.08.008>
- 32 Grant, T., Rohou, A. and Grigorieff, N. (2018) cisTEM, user-friendly software for single-particle image processing. *eLife* **7**, e35383 <https://doi.org/10.7554/eLife.35383>
- 33 Tang, G., Peng, L., Baldwin, P.R., Mann, D.S., Jiang, W., Rees, I. et al. (2007) EMAN2: an extensible image processing suite for electron microscopy. *J. Struct. Biol.* **157**, 38–46 <https://doi.org/10.1016/j.jsb.2006.05.009>
- 34 Pettersen, E.F., Goddard, T.D., Huang, C.C., Couch, G.S., Greenblatt, D.M., Meng, E.C. et al. (2004) UCSF chimera—A visualization system for exploratory research and analysis. *J. Comput. Chem.* **25**, 1605–1612 <https://doi.org/10.1002/jcc.20084>
- 35 Emsley, P. and Cowtan, K. (2004) Coot: model-building tools for molecular graphics. *Acta Crystallogr. D Struct. Biol.* **60**, 2126–2132 <https://doi.org/10.1107/S0907444904019158>
- 36 Niwa, S., Yu, L.-J., Takeda, K., Hirano, Y., Kawakami, T., Wang-Otomo, Z.-Y. et al. (2014) Structure of the LH1–RC complex from *Thermochromatium tepidum* at 3.0 Å. *Nature* **508**, 228–232 <https://doi.org/10.1038/nature13197>
- 37 Evans, M.B., Cogdell, R.J. and Britton, G. (1988) Determination of the bacteriochlorophyll:Carotenoid ratios of the B890 antenna complex of *Rhodospirillum rubrum* and the B800–850 complex of *Rhodobacter sphaeroides*. *Biochim. Biophys. Acta Bioenergetics* **935**, 292–298 [https://doi.org/10.1016/0005-2728\(88\)90224-1](https://doi.org/10.1016/0005-2728(88)90224-1)
- 38 Katz, J.J., Strain, H.H., Harkness, A.L., Studier, M.H., Svec, W.A., Janson, T.R. et al. (1972) Esterifying alcohols in the chlorophylls of purple photosynthetic bacteria. A new chlorophyll, bacteriochlorophyll (gg), all-trans-geranylgeranyl bacteriochlorophyllide a. *J. Am. Chem. Soc.* **94**, 7938–7939 <https://doi.org/10.1021/ja00777a054>
- 39 Hiraishi, A. and Hoshino, Y. (1984) Distribution of rhodoquinone in *Rhodospirillaceae* and its taxonomic implications. *J. Gen. Appl. Microbiol.* **30**, 435–448 <https://doi.org/10.2323/jgam.30.435>
- 40 Moriarty, N.W., Grosse-Kunstleve, R.W. and Adams, P.D. (2009) Electronic ligand builder and optimization workbench (eLBOW): A tool for ligand coordinate and restraint generation. *Acta Crystallogr. D Struct. Biol.* **65**, 1074–1080 <https://doi.org/10.1107/S0907444909029436>
- 41 Bruno, I.J., Cole, J.C., Kessler, M., Luo, J., Motherwell, W.D.S., Purkis, L.H. et al. (2004) Retrieval of crystallographically-derived molecular geometry information. *J. Chem. Inf. Comput. Sci.* **44**, 2133–2144 <https://doi.org/10.1021/ci049780b>
- 42 Bruno, I.J., Cole, J.C., Edgington, P.R., Kessler, M., Macrae, C.F., McCabe, P. et al. (2002) New software for searching the Cambridge Structural Database and visualizing crystal structures. *Acta Crystallogr. B* **58**, 389–397 <https://doi.org/10.1107/S0108768102003324>
- 43 Croll, T. (2018) ISOLDE: a physically realistic environment for model building into low-resolution electron-density maps. *Acta Crystallogr. D Struct. Biol.* **74**, 519–530 <https://doi.org/10.1107/S2059798318002425>
- 44 Kim, D.N. and Sanbonmatsu, K. (2019) CryoFIT: user-friendly fitting of high-resolution cryo-EM reconstructions in PHENIX. *Abstracts of Papers of the American Chemical Society* 257
- 45 Barad, B.A., Echols, N., Wang, R.Y.-R., Cheng, Y., Dimaio, F., Adams, P.D. et al. (2015) EMRinger: side chain directed model and map validation for 3D cryo-electron microscopy. *Nat. Methods* **12**, 943–946 <https://doi.org/10.1038/nmeth.3541>
- 46 Picorel, R., Bélanger, G. and Gingras, G. (1983) Antenna holochrome B880 of *Rhodospirillum rubrum* Sl. Pigment, phospholipid, and polypeptide composition. *Biochemistry* **22**, 2491–2497 <https://doi.org/10.1021/bi00279a028>
- 47 Olsen, J.D., Adams, P.G. and Hunter, C.N. (2014) Aberrant assembly intermediates of the RC-LH1-PufX core complex of *Rhodobacter sphaeroides* imaged by atomic force microscopy. *J. Biol. Chem.* **289**, 29927–29936 <https://doi.org/10.1074/jbc.M114.596585>
- 48 Olsen, J.D., Sockalingum, G.D., Robert, B. and Hunter, C.N. (1994) Modification of a hydrogen bond to a bacteriochlorophyll *a* molecule in the light-harvesting 1 antenna of *Rhodobacter sphaeroides*. *Proc. Natl Acad. Sci. U.S.A.* **91**, 7124–7128 <https://doi.org/10.1073/pnas.91.15.7124>
- 49 Sturgis, J., Olsen, C.N., Robert, B. and Hunter, C.N. (1997) The functions of conserved tryptophan residues of the core light harvesting complex of *Rhodobacter sphaeroides*. *Biochemistry* **36**, 2772–2778 <https://doi.org/10.1021/bi962524a>
- 50 Lang, H.P., Cogdell, R.J., Takaichi, S. and Hunter, C.N. (1995) Complete DNA sequence, specific Tn5 insertion map, and gene assignment of the carotenoid biosynthesis pathway of *Rhodobacter sphaeroides*. *J. Bacteriol.* **177**, 2064–2073 <https://doi.org/10.1128/jb.177.8.2064-2073.1995>
- 51 Chi, S.C., Mothersole, D.J., Dilbeck, P., Niedzwiedzki, D.M., Zhang, H., Qian, P. et al. (2015) Assembly of functional photosystem complexes in *Rhodobacter sphaeroides* incorporating carotenoids from the spirilloxanthin pathway. *Biochim. Biophys. Acta* **1847**, 189–201 <https://doi.org/10.1016/j.bbabi.2014.10.004>
- 52 Chen, J.-H., Wu, H., Xu, C., Liu, X.-C., Huang, Z., Chang, S. et al. (2020) Architecture of the photosynthetic complex from a green sulfur bacterium. *Science* **370**, eabb6350 <https://doi.org/10.1126/science.abb6350>
- 53 Gisriel, C.J., Azai, C. and Cardona, T. (2021) Recent advances in the structural diversity of reaction centers. *Photosynth. Res.* <https://doi.org/10.1007/s11120-021-00857-9>
- 54 Şener, M.K., Strümpfer, J., Hsin, J., Chandler, D., Scheuring, S., Hunter, C.N. et al. (2011) Förster energy transfer theory as reflected in the structures of photosynthetic light harvesting systems. *ChemPhysChem* **12**, 518–531 <https://doi.org/10.1002/cphc.201000944>
- 55 Gall, A., Sturgis, J.D., Fowler, G.J.S., Hunter, C.N. and Robert, B. (1997) The influence of the protein binding site on the absorption properties of the monomeric bacteriochlorophyll in *Rhodobacter sphaeroides* LH2 complex. *Biochemistry* **36**, 16282–16287 <https://doi.org/10.1021/bi9717237>
- 56 Swainsbury, D.J.K., Faries, K.M., Niedzwiedzki, D., Martin, E.C., Flinders, A.J., Canniffe, D.P. et al. (2019) Engineering of B800 bacteriochlorophyll binding site specificity in *Rhodobacter sphaeroides* LH2. *Biochim. Biophys. Acta Bioenergetics* **1860**, 209–223 <https://doi.org/10.1016/j.bbabi.2018.11.008>
- 57 Walz, T. and Ghosh, R. (1997) Two-dimensional crystallization of the light-harvesting L-reaction centre photounit from *Rhodospirillum rubrum*. *J. Mol. Biol.* **265**, 107–111 <https://doi.org/10.1006/jmbi.1996.0714>
- 58 Pettersen, E.F., Goddard, T.D., Huang, C.C., Meng, E.C., Couch, G.S., Croll, T.I. et al. (2021) UCSF ChimeraX: structure visualization for researchers, educators, and developers. *Protein Sci.* **30**, 70–82 <https://doi.org/10.1002/pro.3943>